Article

Multiple Axes of Visual Symmetry: Detection and Aesthetic Preference

Maria Pombo [1,2], Hassan Aleem [1,3,4] and Norberto M. Grzywacz [1,3,4,5,*]

1   Graduate School of Arts and Sciences, Georgetown University, Washington, DC 20057, USA;
    mp5561@nyu.edu (M.P.); ha438@georgetown.edu (H.A.)
2   Department of Psychology, New York University, New York, NY 10003, USA
3   Interdisciplinary Program in Neuroscience, Georgetown University, Washington, DC 20057, USA
4   Department of Molecular Pharmacology and Neuroscience, Loyola University Chicago,
    Chicago, IL 60153, USA
5   Department of Psychology, Loyola University Chicago, Chicago, IL 60660, USA
*   Correspondence: norberto@luc.edu

Abstract: Little is known about the detection of and preference for multiple simultaneous parallel axes of symmetry. Neuroscientists have suggested that the detection of symmetry occurs in extrastriate brain areas with large receptive fields. Such large receptive fields may potentially hinder the simultaneous detection of more than one axis of symmetry. In contrast, psychophysicists have found that symmetry detection occurs within small spatial windows, allowing for the concurrent detection of multiple axes of symmetry. Using psychophysical and computational methods, we aim to test whether multiple axes of symmetry can be detected in parallel and to understand the role of multiple axes of symmetry on aesthetic valence. Experiment 1 provides evidence that multiple axes of symmetry cannot be detected simultaneously. However, with relatively long temporal integration, people can detect them. Experiment 2 suggests that multiple axes of symmetry tend to increase preference. However, the preference for symmetry is not universal because, although most people prefer symmetry, others prefer complex images without axes of symmetry. We present and test a computational model that explains the results of these experiments.

Keywords: symmetry perception; aesthetic preference; processing fluency; temporal integration

1. Introduction

Symmetry is ubiquitous in both nature and art. Although various types of symmetry exist, humans and animals are particularly sensitive to vertical bilateral symmetry [1–3]. Therefore, not surprisingly, ample research has shown that vertical bilateral symmetry is a preferred aesthetic feature (see for a review, [4]) and this preference prevails across cultures, testing contexts, and stimulus types [5]. Thus, finding symmetrical artwork is commonplace [6], with artists often exhibiting a bias towards including symmetry in their paintings [7].

To date, most studies on vertical bilateral symmetry and perception have focused on single axes of symmetry; however, a single image can include many. For example, even if the façade of a house is not symmetrical, it can have embedded vertically bilaterally symmetric axes in its windows, doors, and surroundings. Such multiple axes have been said to implement local symmetry [8]. Can humans detect such multiple axes of symmetry in parallel or is the detection process serial [9–11]? Wagemans and colleagues showed that the ability to detect symmetry increases as the number of axes of symmetry grows [8,12]. However, whether people are seeing multiple axes or simply detecting one axis more easily remains unknown.

Two series of findings raise conflicting answers to this question on symmetry perception. On one hand, the brain regions dedicated to symmetry perception may not be

ideal for the parallel detection of multiple axes of symmetry. For example, Sasaki and colleagues [13] determined that symmetry activates high-order visual areas (V3A, V4, V7, and the lateral occipital complex) (see also [14]). Others have determined that the occipital face area (OFA) responds to the presence of symmetry, even in dot patterns [15,16]. These brain areas involved in symmetry processing are all extrastriate visual areas [17–19]. In such areas, receptive fields tend to be large [20,21]. Such large receptive fields may not be conducive to the parallel detection of multiple axes of symmetry. Large receptive fields may integrate multiple axes of symmetry together, conflating them. Support to the idea that multiple axes of symmetry may not be detected in parallel comes from a study of symmetry and selective attention [22].

On the other hand, large receptive fields are not immediate evidence against the parallel processing of multiple axes of symmetry. For example, the visual system perceives multiple faces of people simultaneously. This occurs, despite large face-processing receptive fields [20]. Moreover, symmetry may not be a property represented in the receptive fields of single neurons. Instead, symmetry may arise at the level of a neural population [23]. Thus, a downstream region could possibly detect multiple axes of symmetry metry in parallel through different readouts from the same population activity. Furthermore, previous psychophysical studies have shown that the spatial extent required to observe symmetry may be small in some conditions [24], but see [25]. The defining property of symmetry is restricted to elements within about $\pm 0.5°$ of the symmetry axis (although the full range of the skirts of the functions are larger). Hence, psychophysical evidence suggests that detecting multiple axes of symmetry in parallel seems plausible, given that humans have close to a 210° forward-facing horizontal arc of visual field [26,27]. The first aim of this study is to elucidate whether humans can detect multiple axes of symmetry with ease.

Another important question related to parallel multiple vertical axes is whether their number influences aesthetic preference. At the most basic level, one can ask, "if people like seeing images with one axis of symmetry, would they not like them more with additional axes?" A reason to suspect that the answer to this question may be positive is the processing fluency theory [7,28,29]. This theory states that an individual's aesthetic response to a stimulus depends on the ease of processing of such a stimulus. If the brain detects multiple axes of symmetry in parallel, it is performing this computation with ease. Thus, the processing fluency theory would apply to how the brain detects multiple axes of symmetry. The second aim of this study is to probe the effect of multiple symmetry axes on aesthetic preference.

Accordingly, we present the findings of two experiments and a computational model on multiple axes of symmetry. In our first experiment, we tested whether subjects could detect two axes of symmetry fluently. We performed the test by asking them to categorize dot patterns containing one or two embedded symmetry axes at different times of exposure. Our second experiment used the same stimuli and ones that contained zero axes of symmetry. However, instead of identifying the number of symmetry axes, participants picked the preferred of two different dot patterns. After presenting these experimental results, we describe a computational model that accounts for the most puzzling aspects of the data. We test this model with a new, independent experiment.

2. Experiment 1

2.1. Materials and Methods

2.1.1. Participants

Ten participants participated in Experiment 1 on multiple-axes-of-symmetry detection (6 females, 4 males, aged 18 to 60 years old), each taking approximately 38 min, on average, to complete the experiment. All participants provided their consent and received payment for participating. For this experiment, participants were recruited using Prolific (https://www.prolific.co/ accessed on 12 June 2020), an online participant recruitment platform. Only participants based in the United States and who had previously indicated

to have normal or corrected-to-normal vision could participate. This and all subsequent experiments were approved by the Georgetown University Institutional Review Board.

We determined the size of the participant cohort with a power analysis. Cohen's *h* is an appropriate measure of effect size between proportions [30]. We were mostly interested in the effect size of the difference in proportion correct for the one-second condition. In this condition, there were 90 observations per participant. To ensure the appropriateness of our sample size, we calculated the smallest possible *h* value that we could obtain assuming $\alpha = 0.01$ and at 0.9 power, using the "pwr" package in R [31]. With a sample size of 10 participants, the smallest possible *h* value was 0.13, which was smaller than what was considered a "small" effect size (though see [32]). Hence, we believed ten participants was a proper sample size to detect an effect.

2.1.2. Apparatus and Stimuli

We programmed the experiment using the Builder view of PsychoPy3 version 2020.1.0 [33]. The experiment was later uploaded to Pavlovia.org (https://pavlovia.org/) to be distributed to participants through Prolific. We administered the experiment consent form and demographic questions through Qualtrics (https://www.qualtrics.com/). Since we conducted the experiment online, all participants used their own devices to complete the experiment. The experiment only worked on computers, and not a smartphone or tablet. Because we could not control the device, we did not have the exact means to measure the visual angle occupied by the stimuli. However, we could estimate it as follows: if a subject typically sat 1 m away (as instructed) from a 27″ monitor with a resolution of 227 ppi, the stimuli would occupy approximately 4.9 × 3.2 degrees of visual angle. If, instead, the subject used a 15″ laptop with full high definition, the stimuli would occupy 7.8 × 5.1 degrees of visual angle. The JavaScript code for Experiment 1 and all subsequent experiments can be found here: https://osf.io/xaekp/.

Because our experimental stimuli were different from the ones used in Tyler's study [24], we conducted a pilot experiment to test whether our stimuli would produce similar results (see S1 Supplementary Materials). This preliminary study showed that single embedded symmetry axes could be detected rapidly. Furthermore, as eccentricity of the embedded axis increased, detection was more difficult (Figure S1). These results are in accordance with Tyler's [24] results and therefore ensure that our stimuli are appropriate for further studies.

For Experiment 1, two types of stimuli were created using the "matplotlib" library of Python [34]: stimuli with one embedded axis of symmetry and stimuli with two embedded axes of symmetry. All stimuli had the same size, a resolution of 72 dpi, and contained the same dot density. They also contained a fixation point in the middle. Figure 1A,B illustrates the two types of stimuli.
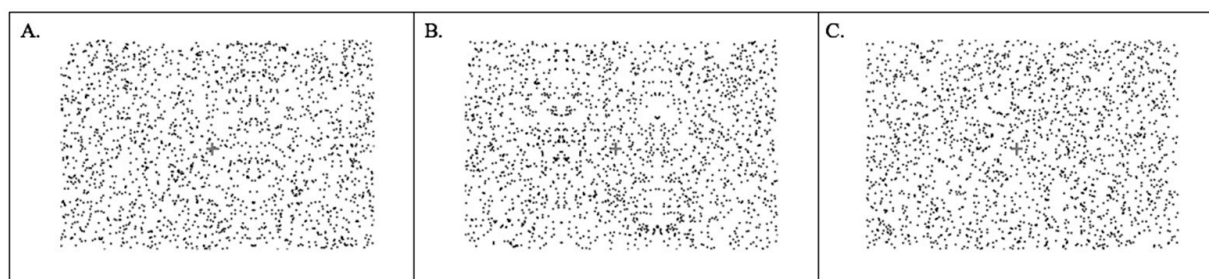

Figure 1. Stimuli. (**A**) Example of the stimuli with one embedded axis of symmetry. (**B**) Example of the stimuli with two embedded axes of symmetry. (**C**) Example of the random dot-pattern stimuli. Masks resembled these latter stimuli, except that masks did not include a fixation point (+).

To generate the stimuli with one embedded axis of symmetry, the whole plot was divided into 13 separate columns. We selected two consecutive columns randomly to include the embedded axis, while the rest of the columns contained randomly generated dots. To create the axis, an algorithm generated random dots in one of the selected columns.

The subsequent column was populated with a set of dots that were vertically symmetrical to the adjacent selected column. The stimuli with two embedded axes of symmetry were created using a similar algorithm. However, this time, two non-touching sets of subsequent columns were selected to include vertically symmetrical axes. Stimuli with one embedded axis of symmetry varied in eccentricity. Stimuli with two embedded axes of symmetry varied in the distance between the two axes (distance), and the distance between the fixation and middle points between the axes (position). For Experiment 1, we only generated stimuli with distances 2, 4, and 6 columns away from the fixation point. (If a subject sat 1 m away from a 27″ monitor with a resolution of 227 ppi, these distances would be approximately 1.14°, 2.28°, and 3.42° degrees of visual angle. If instead the subject used a 15″ laptop with full high definition, then the distances would be 1.82°, 3.64°, and 5.46° degrees of visual angle.) In turn, the positions of the stimuli were 0.5, 1.5, and 2.5 columns. Masking stimuli were created by generating dots with random abscissas and ordinates (Figure 1C), constraining the density to be equal. The code used to generate the stimuli for this experiment and all subsequent experiments can be found here: https://osf.io/xaekp/.

The experiment included 360 stimuli: 180 with 1 embedded axis and 180 with 2 embedded axes (20 for each position and distance combination). Half of the stimuli were presented for 1 s and half for 300 ms.

2.1.3. Procedure

After providing their consent and answering age and gender demographic questions on a Qualtrics survey, the participants received a Pavlovia link to perform the experiment. Before starting, we asked the participants to increase the brightness of their computer screens to their maxima and sit approximately 1 m away from the screens. Participants were instructed that they would see a series of images and would be asked to determine whether these contained one or two axes of symmetry. Subsequently, Experiment 1 included a training period in which participants received feedback on whether they answered questions correctly. Each trial of the experiment started with a fixation point in the center of the screen for 1 s. Then, a stimulus appeared for either 1 s or 300 ms. At the end of the trial, a random-dot mask appeared, and participants indicated whether the previous stimulus contained one or two embedded symmetry axes. Figure 2A provides a graphical representation of the trials. The whole experiment consisted of 366 trials (6 practice trials and 360 experimental ones). The order of the trials was randomized.

2.1.4. Data Analysis

To test whether participants could detect multiple axes of symmetry, we conducted exact binomial tests [35]. To test the effects of time, position, and eccentricity on the detection of multiple axes, we conducted a chi-squared goodness-of-fit test. All data and tests for this and all subsequent experiments can be found here: https://osf.io/xaekp/.

2.2. Results

The first question that we addressed in this paper was whether people could detect multiple axes of symmetry rapidly. We also probed the eccentricity dependence of this putative detection and its dependence on the distance between the axes of symmetry. For this purpose, we probed how well subjects could discriminate images with one axis of symmetry from those with two. These axes of symmetry were embedded in random noise to make the task difficult. Figure 3 displays the results of this experiment for the detection of multiple axes of symmetry.
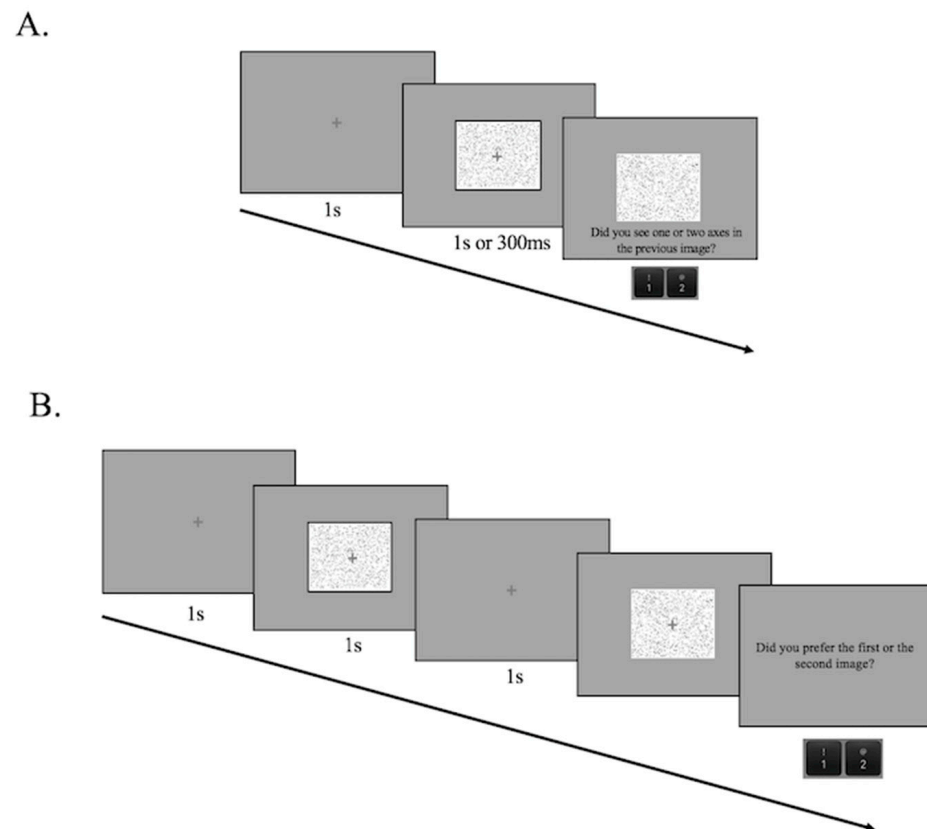
Figure 2. Graphical representation of experiments. (**A**) Procedure of Experiment 1. (**B**) Procedure of Experiment 2. The fixation point appears as + and the symbol under que question rectangle indicates the possible answers.
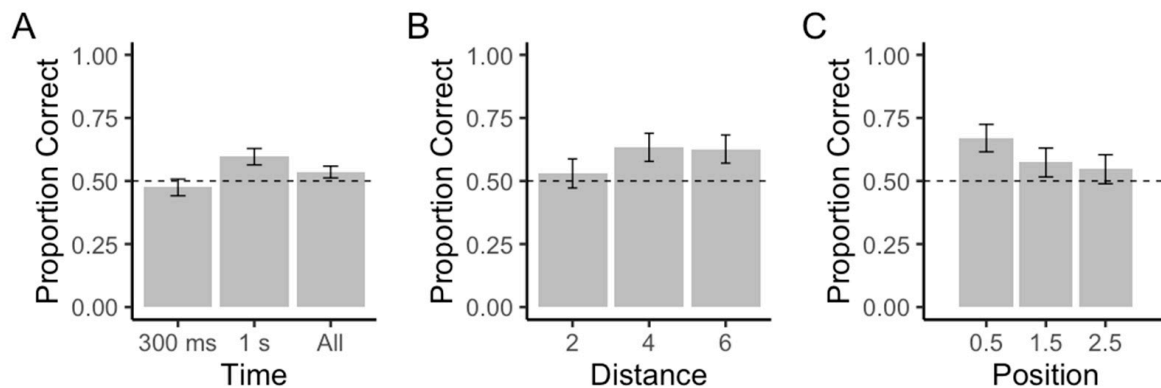

Figure 3. Results of Experiment 1. (**A**) Proportion of correct answers for 2-axes images for different durations of viewing. (**B**) Dependence on the distance between the axes with 1 s presentations. (**C**) Dependence on the position of the axes with 1 s presentations. Distances and positions are measured in terms of columns in our display (see Section 2.1.2 for calibrations in terms of visual angle). The error bars in (**A**) represent 95% confidence intervals using an exact binomial test. The dashed lines in this panel represents chance. In turn, the error bars in (**B**,**C**) represent ± 2 standard errors and the dashed lines represent the expected proportion correct without an effect of eccentricity or distance effect. Subjects were at chance if the presentation was 300 ms long but were above chance with 1 s exposures. Eccentricity and distance had no statistically significant effect on performance.

To probe whether people could detect multiple axes of symmetry, we tested different null hypotheses. The first was that no observer performed better than chance. If we rejected this null hypothesis, we would show that some observers could detect two symmetry axes.

Because the hypothesis assumed that all observers were at chance, they formed a single population whose samples should have behaved as binomial distributions with a success probability of 0.5. We thus performed exact binomial tests. We detected no difference from chance when presenting stimuli for 300 ms (first bar in Figure 3A). However, when the stimuli were presented for 1 s (second bar in Figure 3A), at least some subjects performed statistically significantly above chance ($p < 0.007$). We then used a chi-squared test to confirm that the performance at 1 s was statistically significantly better than at 300 ms ($\chi_1^2 = 12.3$ (with Yate's continuity correction), $p < 0.0005$). These results showed that at least some subjects could distinguish two axes of symmetry from one when the observation time was long enough. To what degree were these results valid across individuals? To answer this question, we repeated these tests for each individual separately. When performing the binomial exact test for being above chance ($p < 0.05$), only one individual out of ten passed the probe with 300 ms. In contrast, six individuals out of 10 passed it for 1 s. The performance was better at 1 s than at 300 ms for all individuals, with the difference being significant for six out of ten individuals (two-sample binomial test, $p < 0.05$). Thus, most subjects could detect multiple axes of symmetry at presentation times of 1 s, but not 300 ms.

Finally, based on a χ^2 goodness-of-fit analysis, our results do not suggest an effect of eccentricity on the detection of multiple axes (Figure 3B). Similarly, our results do not suggest an effect of distance on this detection (Figure 3C).

2.3. Discussion

The results from Experiment 1 suggest that individuals cannot detect multiple vertical axes of symmetry with ease, and such detection requires long temporal integration. Thus, the ability to detect multiple axes of symmetry appears to depend on slower mechanisms. These slow mechanisms may involve saccades [36] or shifting of attention [37]. This slow detection of multiple axes of symmetry suggests that if people prefer them to single axes, then we require an explanation beyond the framework of the processing fluency theory.

3. Experiment 2

3.1. Materials and Methods

3.1.1. Participants

Twenty-five new participants participated in Experiment 2 (13 females, 11 males, 1 other, aged 18 to 58 years old). It took each participant approximately 31 min, on average, to complete the new experimental procedures. All participants provided their consent to participate in the experiment and received payment for participating. They were again recruited using Prolific (accessed on 23 July 2020).

We again determined the size of the participant cohort with a power analysis. For our second experiment, we were mostly interested in the effect size of the difference in proportion preferred in the one-versus-two axes condition. In this condition, there were 60 observations per participant. With a sample size of 25, and assuming $\alpha = 0.01$ and at 0.9 power, the smallest possible observable value for Cohen's h was 0.1. This value was again smaller than what was considered a "small" effect size. Hence, we believe that twenty-five participants is a proper sample size to detect an effect.

3.1.2. Apparatus and Stimuli

Experiment 2 was programmed and distributed in the same way as Experiment 1, and the same stimuli used in Experiment 1 were used in Experiment 2. Additionally, we used a third type of stimuli consisting of completely random dot patterns (Figure 1C). For the stimuli consisting of two embedded symmetry axes, we chose a fixed position (0.5) and a fixed distance (4). These values corresponded to the highest proportion correct for 1 s in Experiment 1. These parameters limited the choices of columns that we could select for the symmetry axes. Thus, the stimuli consisting of one embedded symmetry axis only included symmetry axes in those columns. Figure 1 shows the three types of stimuli used.

The experiment included 480 stimuli: 160 random, 160 with 1 embedded axis, and 160 with 2 embedded axes, with each stimulus presented for 1 s.

3.1.3. Procedure

After providing consent, the participants completed the same demographic survey as in Experiment 1. They then received the same instructions regarding brightness and distance from the screen. Participants were then instructed that they would see two images and would be asked to select which one they preferred. Because the questions had no right answers, Experiment 2 did not include training. However, to allow participants to acquaint themselves with the experiment, we included a few test trials at the beginning, not included in the analysis. Each trial of the experiment started with a fixation point at the center of the screen for 1 s. Then, the 1st image appeared for 1 s, another fixation point appeared for 1 s, and the 2nd image appeared for 1 s. Participants were asked whether they preferred the first or second image. Figure 2B shows a graphical representation of a trial of the procedure seen by the participants. The experiment consisted of 249 trials. They comprised 9 practice trials, 60 trials of each combination of stimuli (zero vs. one axis, one vs. two axes, and zero vs. two axes), and 20 trials of pairs of the same stimuli (zero vs. zero, one vs. one, and two vs. two axes) to ensure that order did not influence preference. The order of the trials was random and the order of the combinations counterbalanced.

3.1.4. Data Analysis

All analyses were conducted in R Studio (R version 4.0.5). We conducted a series of exact binomial tests for each possible combination of stimuli [35]. We performed these tests both at the group and individual levels. Additionally, to test the consistency of responses for participants, we calculated the Pearson's correlation coefficients and tested the significance of the correlation of each combination of conditions (zero vs. one axis, one vs. two axes, and zero vs. two axes).

3.2. Results

From the results of Experiment 1, we know that people cannot detect multiple axes of symmetry rapidly. A long-temporal integration window is required for the detection of these axes. Therefore, if we assume that the processing fluency theory is the main explanation for aesthetic biases, then we should predict that multiple axes of symmetry may not make a difference. To test this prediction, we designed Experiment 2 to compare the aesthetic preferences elicited by one versus two axes of symmetry. The outcome of this experiment appears in Figure 4.

To understand the participants' preferences for multiple axes of symmetry, we calculated the number of times they chose the option with the greater number of symmetry axes. Figure 4A shows the results of these choices. The participants significantly chose a greater number of axes in the one-versus-two and the zero-versus-two axes conditions ($p = 0.002$ and $p = 0.007$, respectively). However, the zero-versus-one axes condition yielded no statistically significant difference.

How could seeing two axes of symmetry boost aesthetic preference when seeing one axis did not elicit preference? To answer this question, we decided to look more closely at how each participant responded to multiple axes of symmetry in the task. Figure 4B shows the plot of the difference between the times each participant chose the option with the greater number of axes instead of the option with fewer axes. The vertical lines represent the place where that difference would be significant ($p < 0.005$) in an exact binomial test. Our results show that out of the 25 people that participated in our study, the difference is significant for 15 of them. Furthermore, 9 of the participants significantly preferred a greater number of symmetry axes. In contrast, 6 participants significantly preferred a reduced number of symmetry axes. These results suggest that, when it comes to preference, symmetry matters. However, whether symmetry increases or decreases preference appears to be participant dependent.
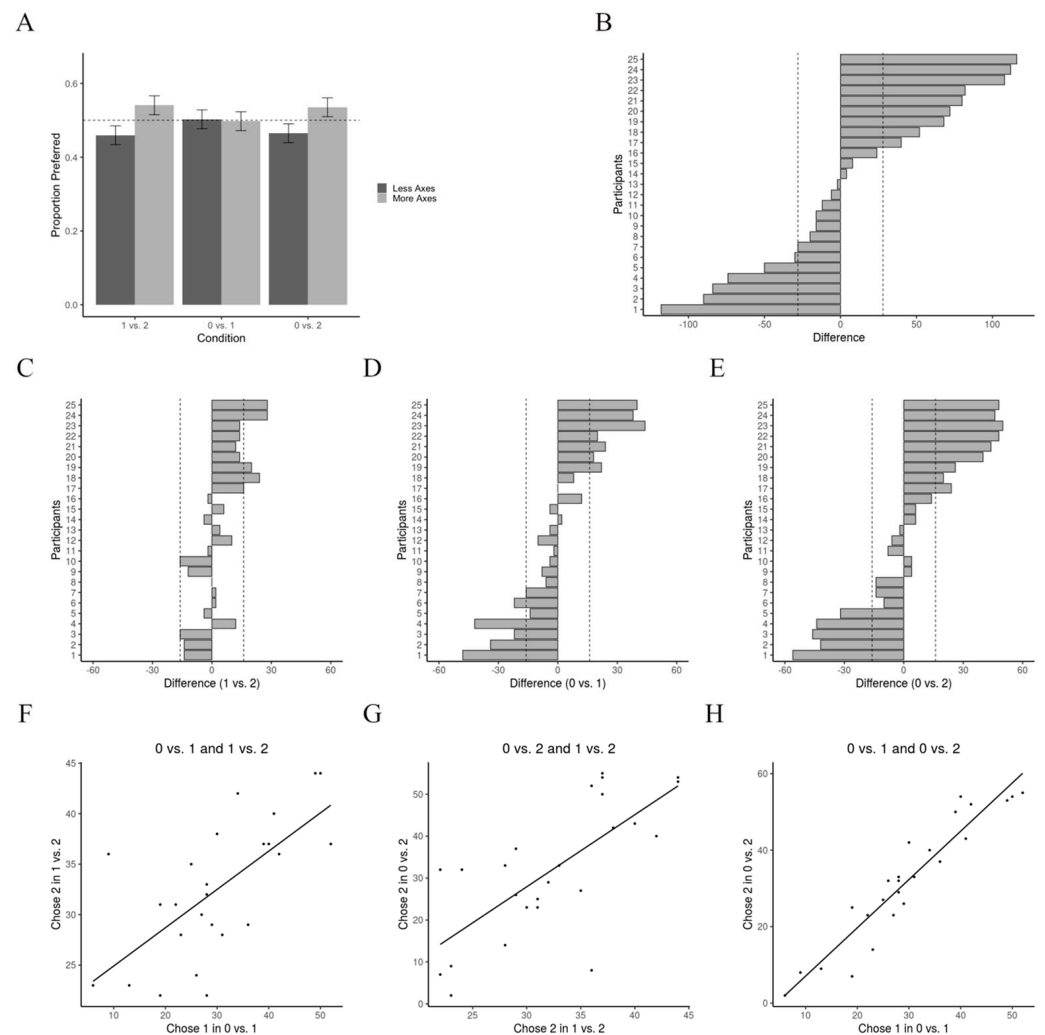
Figure 4. Results of Experiment 2. (**A**) Exact binomial test results comparing the number of times that participants chose the image with the higher number of embedded symmetry axes versus the option with fewer axes. This figure is a visual representation of the binomial test because the error bars correspond to 95% confidence intervals. Moreover, the dotted lines represent chance preference (50%). If the error bars do not overlap with the 50% line, we can reject the null hypothesis that participants like both images equally. (**B–E**) Graphical representation of individual differences in symmetry preference. (**B**) Pertains to all conditions and (**C–E**) displays all conditions separately. The horizontal axis represents the difference in count between the times that the participant selected the option with more symmetry axes and the times that the participant selected the lesser option. Each difference bar is for one participant, labeled from 1 to 25. Since the difference relies on the raw counts, the differences for the combined conditions are greater than for the individual ones. The dotted lines represent the point where the difference would be significant ($p < 0.05$) for an exact binomial test. (**F–H**) Correlation between the times that the participant chose the option with the largest number of embedded axes across different conditions. The main conclusion is that two axes of symmetry yield more aesthetic preferences than one axis.

This split preference for symmetry in the population might help explain why one axis of symmetry embedded in complex noise did not elicit preference. Perhaps this split was balanced enough in the population. To test this prediction, we broke Figure 4B into the difference for each participant for each condition. Figure 4C–E shows the plots for each condition and participant. As predicted, when judging zero-versus-one axes of symmetry, 7 participants preferred symmetry while 5 preferred not to have symmetry embedded in

the noise (Figure 4D). These numbers were so close that our sample did not yield evidence for a population preference for symmetry or for a purely complex random pattern.

Thus, why does preference for symmetry increase when we increase the number of axes of symmetry (Figure 4A)? Comparing Figure 4D with Figure 4E shows that the number of people preferring patterns with symmetry increases from 7 to 9 when we increase the number of axes from 1 to 2. The intensity of preference also increases. In contrast, the number of people preferring non-symmetry stays constant (5), and the intensity of preference increases less on average. Hence, our data indicate that more people prefer symmetry than prefer its absence in a complex random pattern.

We also wanted to test the preference consistency of participants. Thus, we tested whether those who liked symmetry (or non-symmetry) with one axis still preferred symmetry (or non-symmetry) with multiple axes. We calculated the correlations between the number of times a participant chose the greater number of axes across pairs of conditions (Figure 4F–H). The results of our Pearson's correlation tests suggest a strong, positive, linear correlation between the individuals that chose the greater number of axes. For the zero-versus-one and one-versus-two axes pair, the statistics were $r = 0.94$, $p < 0.001$. For the zero-versus-one and one-versus-two axes pair, the statistics were $r = 0.78$, $p < 0.001$. Lastly, for the zero-versus-two and one-versus-two axes pair, the statistics were $r = 0.8$, $p < 0.001$. This positive correlation indicated that if participants liked symmetry with one axis, they preferred symmetry with multiple axes. If participants preferred non-symmetry, they also preferred non-symmetry with multiple axes.

Lastly, as a control, we checked whether preferences were split 50–50 for equal-num number-of-axes conditions. Binomial tests indicated that preference was not significantly different for the first-versus-second images in zero-versus-zero ($p > 0.39$), one-versus-one ($p > 0.75$), and two-versus-two ($p > 0.34$) controls, suggesting no-order effects.

3.3. Discussion

Our results reveal two main findings for Experiment 2. First, while some people prefer to see axes of symmetry embedded in the complex random-dot image, others prefer the opposite (Figure 4B–E). Second, multiple axes of symmetry elicit greater aesthetic preference on average in the population (Figure 4A,D,E). A possible explanation for the first finding stems from increases in symmetry or balance reducing the complexities of images [7,38]. Previous research looking at individual differences in aesthetic preferences for complexity [39] showed that some participants liked complexity while others disliked it [7,40,41].

4. A Theoretical Framework for the Detection and Preference of Multiple-Symmetry Axes

4.1. Assumptions

The results of Experiment 1 indicated that seeing two axes of symmetry embedded in a random-dot pattern takes time. Moreover, the results of Experiment 2 indicated that people who liked symmetry preferred more of it. Given our results, we hypothesized that multi-axis preference depended on temporal integration, and thus proposed how to model it.

The simplest hypothesis for why multiple axes of symmetry increase aesthetic preference makes four assumptions:

1. Seeing symmetry is detecting at least one axis of symmetry, and sensing more axes makes no difference.
2. As the number of axes of symmetry increases, the probability of detecting at least one of them also increases. Thus, the probability of detecting at least one axis of symmetry follows probability summation [42].
3. When confronted with a choice between symmetry or complexity, each individual has a consistent preference for either the former or latter. However, these judgments are likely influenced by noise, ranging from the nature of the stimuli to decision noise, and thus are not absolute.

4. If an individual fails to detect symmetry in the two experimental images, preference is random.

In Experiment 3, we describe a within-participant procedure designed to test these theoretical assumptions. In the first part of the experiment, we measure how well observers can detect axes of symmetry when they have different degrees of noise. We start with images with just one of these axes. From this measurement, we then test Assumptions 1 and 2 by performing a similar detection experiment; however, presently, with two axes of symmetry. From our data, we can calculate a psychometric detection curve as a function of stimulus noise. From Assumptions 1 and 2, we can predict the shape of the detection curve with two axes from the detection curve with one axis. Then, we use the same stimuli to probe preference for these images as compared to images with no axes of symmetry. From Assumptions 3 and 4, we can predict the preference curves from the detection ones.

4.2. Experiment 3—Test of the Assumptions of the Theoretical Framework

4.2.1. Methods

Eleven new subjects participated in Experiment 3 (7 females and 4 males, aged 21 to 50 years old). Each participant completed two sessions and took approximately 60 min, on average, to complete each session. Participants completed the second session between 24 and 48 h after the first session. All participants provided their consent to participate in the experiment and received payment for participating. They were again recruited using Prolific (accessed on 19 January 2022).

For this experiment, we created a variation of the stimuli in Experiments 1 and 2. We re-created stimuli with one or two symmetrical axes introducing a new noise variable: the proportion of dots within the axis that were symmetrical. A proportion of zero meant that all the points in the axis were completely random, and the stimulus was identical to the random-dot stimuli in Experiment 2. A proportion of 1 meant that all the points in the axis were symmetrical, analogous to the one- and two-axes stimuli we used in previous experiments. The proportion of symmetrical dots per symmetry axis in our stimuli varied linearly from 0.4 to 1 in units of 0.05. This meant that for each type of stimulus (one- and two-axes), we had 13 different levels of proportion of symmetry. All other variables, such as the distance and position of the symmetrical axes and the density of the dots, were identical to those in Experiment 1.

Participants completed this experiment in two sessions. The first session was a preference task, like the one in Experiment 2. The second session was a detection task, like the one in Experiment 1. Each session had 520 trials. Half of them required making a judgment between random and one-axis stimuli and half of them between random and two-axes stimuli. We randomized the order of the trials and counterbalanced the presentation of the stimuli within each trial.

After providing consent, the subjects participated in the first session of the experiment. First, the participants answered demographic questions and obtained the same instructions regarding screen brightness and sitting distance as the participants in all previous experiments. Each trial started with a one-second fixation cross. Then, the participants saw two stimuli, each for one second (separated by a one-second inter-stimulus interval). Subsequently, they were asked to use their keyboards to indicate which of the stimuli they preferred. The second session was analogous to the first session, except the participants were asked which of the two stimuli contained an axis of symmetry. Importantly, even if the stimuli contained two axes of symmetry, the participants only had to indicate whether it contained at least one. This session started with six practice trials (which were excluded from the analysis), for which participants received direct feedback on whether they answered the questions correctly. All participants completed the two sessions in the same order to avoid the detection task biasing their preferences.

All our data analyses were conducted in R. We were interested in calculating percent correct as a function of the proportion of symmetry. For the detection session, for each condition, we fitted a psychometric curve by calculating the cumulative normal that

minimized the negative log likelihood using two parameters: a threshold and a sigma. To obtain the best fit, we used the "optim" function in R. We used the best-fit 75% threshold and sigma of the psychometric curves to predict the psychometric curves of the preference session, and we used a chi-squared goodness-of-fit test to assess how our predictions fitted the data. The equations and details of our predictions are described below (computational model for testing assumptions of framework).

4.2.2. Results

From the assumptions of the theoretical framework, two main predictions arise: first, the detection of symmetry in images with multiple axes of symmetry follows probability summation; second, preference is determined by the detection of at least one axis, such that detecting more does not matter. Experiment 3 tested these two predictions for different subjects, thus also probing the effects of their individual abilities to detect symmetry. The results of this experiment appear in Figure 5, first focusing on detection (panels A–C) and then on preference (panels D–F).

Figure 5A,B show the detection results for two extreme subjects. While the former exhibits a detection increase as the degree of symmetry increases, the latter barely changes. To quantify this difference between subjects, we fitted error functions through the data. Subjects were considered as not detecting axes of symmetry in our experiments if any of their error-function thresholds were higher than one. Of our eleven subjects, five could not detect axes of symmetry. The proportions of subjects who could and could not detect axes of symmetry were compatible with the results in Figure 4D,E. For the subjects that could detect axes of symmetry, the detection curves for two axes (green lines) predicted from the one-axis results (blue) matched closely with what we obtained from the observers (red). To quantify this match, we plotted the predicted thresholds and sigmas (standard deviations) against their observed values (Figure 5C). These plots yielded reasonably good linear fits ($r = 0.68$ and $r = 0.57$ for thresholds and sigmas, respectively), which were statistically indistinguishable from the perfect-match-of-model line. Hence, the fits in panels A–C of Figure 5 supported Assumptions 1 and 2 of our theoretical framework.

The second part of Experiment 3 tested whether subjects' preferences matched the predictions based both on Assumptions 3 and 4 of our theoretical framework, and on results similar to those presented in Figure 5A,B. Figure 5D,E show the preference results for two typical subjects. While the former exhibited an increase in preference as the degree of symmetry increased, the latter showed a decline. The increase was statistically significant for both one- and two-axes experiments (Pearson's $r = 0.57$; $p < 0.05$ for one axis; $r = -0.80$; $p < 0.002$ for two axis). The decline was also statistically significant for the one-axis experiment ($r = 0.65$; $p < 0.02$). However, although the decline was apparent for two axes ($r = -0.47$), it did not cross the statistical threshold. Nevertheless, even for two axes, in 12 out of the 13 times that the subject made a choice, the pick was for the image without symmetry. Consequently, this subject strongly preferred complexity over symmetry (binomial test, $p < 0.002$). Hence, these results are consistent with subjects preferring either symmetry or complexity (Assumption 3). As a population, 3 out of the 6 subjects preferred images with symmetry, whereas 3 preferred complexity. This equal split between subjects was compatible with the numbers presented in Figure 4D,E.

Another result in Figure 5D,E is that the quantitative predictions based on Assumptions 3 and 4 (solid lines) fit the preference data appropriately. A χ^2 test using all the preferences across subjects confirms that the data and predictions are statistically indistinguishable. Splitting the χ^2 test subject by subject also shows that this indistinguishability worked individually (Figure 5F mean $p = 0.98 \pm 0.01$). These tests suggest that the relatively large deviations of the model from the data are due to their noise. Hence, the tests provide further support for the validity of Assumptions 3 and 4 of our theoretical framework.
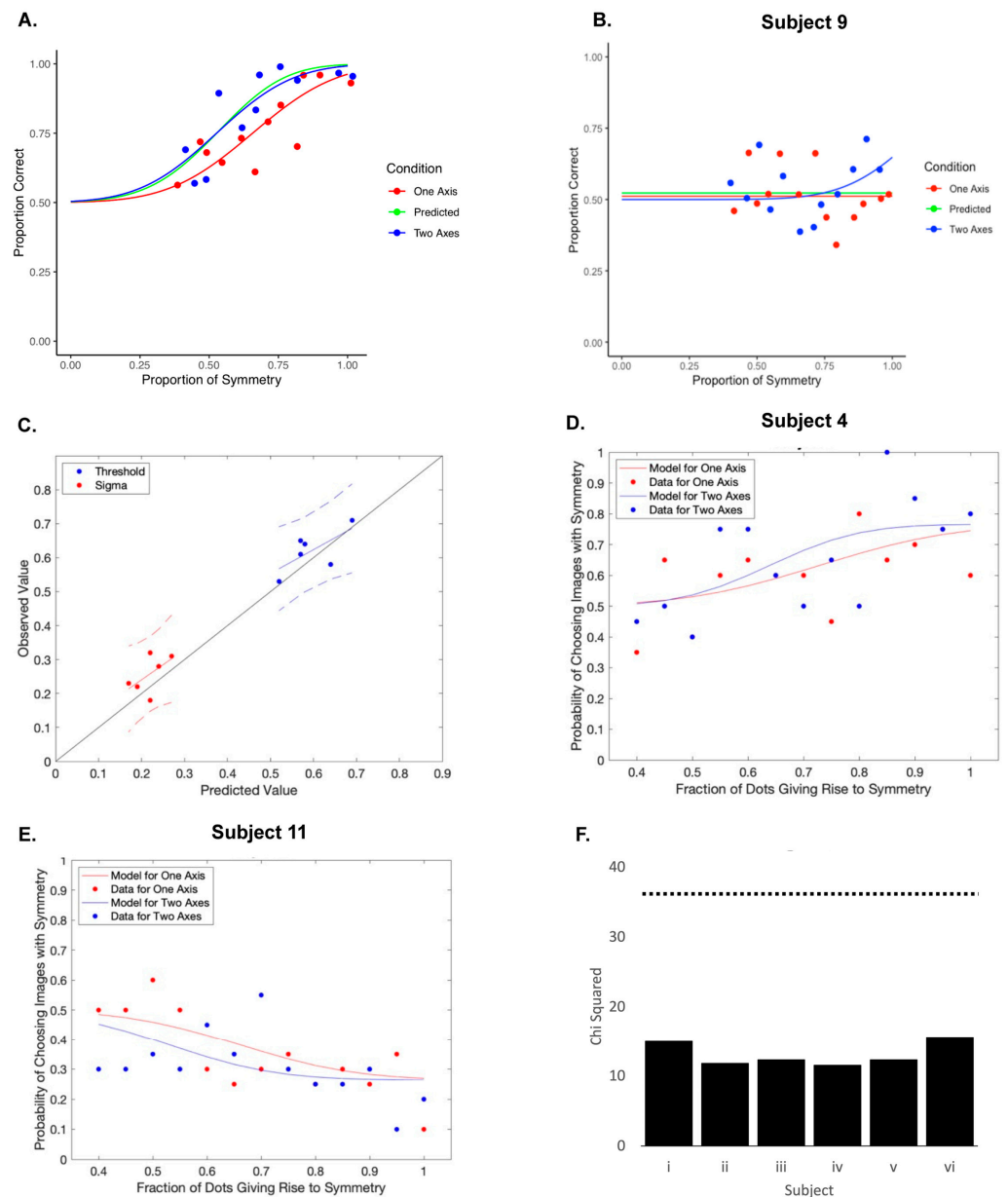
Figure 5. Results of Experiment 3. (**A**,**B**) Examples of subjects able (**A**) and unable (**B**) to detect the axes of symmetry. The dots provide the detection data, while the solid lines with corresponding colors are the best error-function fits. The green lines are the predicted performances for the two-axes experiment given the one-axis results, and Assumptions 1 and 2 (Equation (3)). These lines are close to the two-axes-experiment blue lines. (**C**) Observed (blue lines in (**A**,**B**)) versus predicted (green lines) thresholds and sigmas (standard deviations) for the six subjects capable of detecting axes of symmetry. The solid lines are the best linear-regression results, while the dashed curves indicate the 95% confidence intervals. The regression yield results statistically indistinguishable from the (black) line, marking a perfect match between the results and predictions. Consequently, the results of panels (**A**–**C**) support the hypothesis that subjects detect symmetry in multi-axis experiments by probability summation (Assumption 2). (**D**,**E**) Examples of subjects who prefer (**D**) and do not prefer (**E**) symmetry. The dots provide the mean preference data, while the solid lines with corresponding colors are the best fits of the model (Equation (5)). The parameters of the fits are $\theta = 1$ and $\rho = 0.766$ for panel (**D**), and $\theta = -1$ and $\rho = 0.736$ for panel (**E**). (**F**) Chi-squared values of the fits for the six subjects who could detect the axes of symmetry. These values are lower than the threshold for $p = 0.05$ (χ^2_{24} tests—dotted line), indicating that the model is indistinguishable from the data for every subject.

4.2.3. Discussion

The results in Figure 5 provide a confirmation of the points raised by the theoretical assumptions of our framework. These assumptions imply that some people like symmetry while others do not so much. We can see in Figure 5D that for people who like symmetry, their preference for the symmetric image increases as the symmetry signal in the image increases. Additionally, the opposite occurs for people who dislike symmetry (Figure 5D). These conclusions stand, regardless of whether our computational model (red and blue lines) is right in detail. The same cannot be said for the probability summation results (Figure 5A–C). The arguments for probability summation are quantitative, with the results lending support to this.

4.3. Computational Model for Individual Observers

4.3.1. Rationale

By translating the assumptions raised in our theoretical framework into appropriate equations, we have simulated observers of our experiments. With our assumptions, we can explain many of the complex features in Figures 4 and 5. Some of the features on the processing of axes of symmetry may be intuitive. For example, by presenting two axes of symmetry instead of one, the probability of detecting at least one axis increases. Therefore, if some people like symmetry, they increase the number of times that they like images with axes of symmetry (Figures 4D,E and 5D). Similarly, if some people prefer complexity, they increase the number of times that they like the images without axes of symmetry (Figures 4D,E and 5E). If, instead, we compare images with one versus two axes, the difference decreases (Figure 4C). This is because people may see at least one axis in both images. Consequently, we can qualitatively account for the dependence on the number of axes of symmetry. However, a quantitative analysis is necessary to make the details of this dependence convincing. To quantify the explanations of Figures 4 and 5, we developed a computational model based on the four assumptions of our theoretical framework. Here, we begin the mathematical development with an eye to explain data like those in Figure 5. In this model for testing the assumptions of the proposed theoretical framework, we shift to Figure 4.

4.3.2. Fundamental Equations of the Model

The horizontal axes of Figure 5A,B are the proportion of dots creating symmetry. We denote this by ϕ. The vertical axes are the proportion of times that a subject reports the image with symmetry as having it. We denote this as $P_r(\alpha, \phi)$, where α was the number of axes of symmetry in the target image. To obtain the number of times that a subject reported an axis of symmetry as having it, we multiply this quantity by the number of trials, M_r.

In Figure 5A,B, we modeled $P_r(\alpha, \phi)$ as error functions of ϕ [43]. To probe Assumptions 1 and 2 of our theoretical framework, we compared $P_r(2, \phi)$ with its estimate from $P_r(1, \phi)$, denoted $P_r^{(e)}(2, \phi)$. This estimate was composed of those images for which the subject detected the axis (with probability denoted by $P_d(\alpha, \phi)$) and half of those images for which detection was not possible. Thus,

$$P_r(\alpha, \phi) = P_d(\alpha, \phi) + \frac{1}{2}(1 - P_d(\alpha, \phi)). \tag{1}$$

The choice of half in the second term of this equation was tested in our experiments. Because they involved two alternative-forced choices, the only way that this choice would not hold up was if the order of presentation mattered. However, we controlled for order and it did not influence the responses. False alarms were also conceivable, possibly affecting the first term of Equation (1). However, given the random nature of our images, we assumed that such false alarms were rare and thus had a negligible effect.

From the probability summation, the connection between $P_d(2, \phi)$ and $P_d(1, \phi)$ is

$$P_d(2, \phi) = 1 - (1 - P_d(1, \phi))^2. \tag{2}$$

In this equation, $1 - P_d$ refers to the probability of failing to detect. The term is squared to refer to the probability of failing to detect both axes. Therefore, the equation expresses the probability that we do not fail to detect both axes, meaning the probability that we detect at least one. By using Equations (1) and (2), and some algebra, we can eliminate P_d, obtaining

$$P_r^{(e)}(2, \phi) = 1 - 2(1 - P_r(1, \phi))^2. \tag{3}$$

This is the equation that we used to estimate the green lines in Figure 5A,B.

4.3.3. Equations for Individual Preference of Symmetry

We now switch our attention to the preference results in Figure 5D,E. In these figures, the vertical axes are the number of times a subject prefers the image with axes of symmetry. We denote this number by $M_p P_p(\alpha, \phi)$, where M_p is the number of trials, P_p is the probability of preferring the image with symmetry axes. To probe Assumptions 3 and 4 of our theoretical framework, we compare the estimated $P_p^{(e)}(\alpha, \phi)$ with the preference data. This estimate is again composed of the images for which the subject detects the axis and half of the images for which detection is not possible. However, as expressed in Assumption 3, a subject's preference is not absolute. Our images are noisy, which means participants may be detecting other shapes that they find more appealing than symmetrical axes. Alternatively, their preferences may be noisy [44]. Consequently, if a subject detects symmetry and tends to like it, the probability that the individual would pick the symmetrical image is less than 1. We denote this probability with the parameter $0.5 < \rho < 1$. In turn, the parameter θ denotes the tendency to like symmetry ($\theta = 1$) or prefer the opposite image ($\theta = -1$). With these parameters and assumptions in hand, we can write:

$$P_p^{(e)}(\alpha, \phi : \theta, \rho) = \frac{1}{2}(1 - P_d(\alpha, \phi)) + \frac{1 + \theta}{2} \rho P_d(\alpha, \phi) + \frac{1 - \theta}{2}(1 - \rho) P_d(\alpha, \phi), \tag{4}$$

where we use the notation $f(x : k)$ to mean a function of x parametric on k. In this equation, the first term on the right-hand side captures the cases where the subject does not detect the axis of symmetry. In turn, the second term applies for cases where the subject detects an axis and likes it. Thus, $\theta = 1$, making $((1 + \theta)/2 = 1$ and $((1 - \theta)/2 = 0)$. Finally, the third term is for subjects that detect the axis of symmetry and dislike it, that is, $(1 + \theta)/2 = 0$ and $((1 - \theta)/2 = 1$. Some algebra with Equation (4) and the application of Equation (1) provides:

$$P_p^{(e)}(\alpha, \phi : \rho) = \frac{1}{2}(1 + \theta(2P_r(\alpha, \phi) - 1)(2\rho - 1)), \tag{5}$$

This is the equation used to estimate the red and blue lines in Figure 5D,E.

4.3.4. Methods

We obtained the fit of the error functions to data similar to those in Figure 5A,B, for each individual. These fits were separate for the one- and two-axes cases (red and blue curves, respectively). We used robust regression for the fits [45], specifically the Nelder–Mead algorithm [46], with the mean (threshold) and standard deviation (sigma) as free parameters. We then tested the quality of these fits for each curve with χ_{65}^2 tests. The number of degrees of freedom was 65 because we had 6 individuals, with 13 data points per curve and 2 parameters per individual. Then, we calculated the predicted two-axes reporting (Equation (3)—green lines in Figure 5), testing it against the two-axes data (blue dots), also employing χ_{77}^2 tests. These tests had 77 degrees of freedom because they were parameter-free. Finally, we fitted the predicted preference curves (Equation (5)—red and blue lines in Figure 5D,E). The fit optimized the free parameter of the equation individually by minimizing χ_g^2 of the goodness of fit of $P_p^{(e)}(\alpha, \phi : \rho)$ to the equivalent data from Experiment 3 (red and blue dots). The measure χ_g^2 depends on the free parameter of $P_p^{(e)}$, that is, it provides:

$$\chi_g^2 = \chi_g^2(\rho).$$

To find the optimal free parameter, we calculate:

$$\rho^{(opt)} = argmin_\rho \chi_g^2. \tag{6}$$

We perform the minimization specified in this equation with a coordinate descent algorithm [47].

4.3.5. Results

As mentioned in the analysis of Experiment 3, the error-function fits (red and blue curves in Figure 5) were statistically indistinguishable from the data (similarly colored dots). A similar conclusion held for the fits of Equation (3) (green curves and blue dots). The parameters of the fits for the two-axes experiments appeared in Figure 5C. In turn, for the one-axis experiments, the six fits yielded thresholds = (0.74, 0.87, 0.73, 0.71, 0.76, 0.66) and sigma values = (0.30, 0.32, 0.27, 0.27, 0.21, 0.24) for subjects 1–6 in Figure 5F. Finally, the respective optimal parameters of the fits of the green lines were $\theta = (1, -1, 1, -1, 1, -1)$ and $\rho = (0.51, 0.59, 0.77, 0.52, 0.74)$. That $\rho < 1$ is consistent with the second part of Assumption 3 in our framework.

4.3.6. Discussion

The results in this section expand and support those of Experiment 3. Assumptions 1 and 2 of our theoretical framework not only account for the data qualitatively, but also quantitatively. Thus, $P_r(2, \phi)$ and $P_r^{(e)}(2, \phi)$ (Equation (3)) are statistically indistinguishable (Figure 5A–C), in support of Assumptions 1 and 2. A similar result was obtained in relation to Assumptions 3 and 4. In Figure 5D–F, we see that $P_p(\alpha, \phi)$ and $P_p^{(e)}(\alpha, \phi)$ (Equation (5)) are statistically similar. The data in Experiment 3 also show a high degree of individuality. People not only vary widely in their ability to detect axes of symmetry, but also in whether and how much they like them.

4.4. Computational Model for the Population
4.4.1. Rationale

The computational model described above quantified the predictions of our theoretical framework at the individual level. In this section, we modeled Experiment 2 to try to quantify population aspects of the perception and preference of multiple axes of symmetry. We thus aimed to validate the theoretical assumptions further by testing them against the results in Figure 4.

4.4.2. Population Equations

We modeled Experiment 2 by running M simulations for each condition, with N people in each simulation. Following Assumption 3 of our framework, let the mean fraction of people who prefer symmetry versus complexity in the population be f_s. Therefore, the number of participants, $n_i^{(s)}$, in the ith experiment who prefer symmetry follows the binomial probability distribution:

$$P\left(n_i^{(s)} : N, f_s\right) = \binom{N}{n_i^{(s)}} f_s^{n_i^{(s)}} (1 - f_s)^{N - n_i^{(s)}}. \tag{7}$$

Assumption 3 also means that the number of participants who prefer complexity, $n_i^{(c)}$, is:

$$n_i^{(c)} = N - n_i^{(s)}. \tag{8}$$

To use Assumption 3, we must begin by specifying the probability that the *j*th participant in the *i*th experiment detects the axis of symmetry when presented with just one such axis. We do so by generalizing the notation of P_d in Equation (1) to $P_d^{j,i}(\alpha = 1)$. In this

notation, we drop the ϕ parameter for concisiness because, in Experiment 2, $\phi = 1$. With this notation, Assumption 3 is captured by Equation (2) with the i and j indices included:

$$P_d^{j,i}(\alpha) = 1 - \left(1 - P_d^{j,i}(1)\right)^\alpha \tag{9}$$

To implement Assumptions 1 and 4, we must compare two images, with one with at least one axis of symmetry and one without. Each subject performs this comparison L times for each experiment. We thus introduce the notation $D_{j,i}(\alpha_1, \alpha_2)$ to represent the difference of the number of times that the jth participant in the ith experiment prefers the image with α_2 axes of symmetry versus α_1 axes, where $\alpha_1 < \alpha_2$. To calculate $D_{j,i}(\alpha_1, \alpha_2)$, we must use Assumptions 1 and 4. From the latter assumption, if the participant fails to see symmetry in a particular trial, the answer is random. Similarly, the answer is random if the participant sees axes of symmetry in both images (Assumption 1). We approximate those random answers as making no contribution to $D_{j,i}(\alpha_1, \alpha_2)$, which is true on average. Thus, the only contributions to $D_{j,i}(\alpha_1, \alpha_2)$ come from seeing at least one axis of symmetry in one image, but not in the other (Assumption 1; Equation (9)). The contributions are positive if the subject prefers symmetry and sees an axis of symmetry for the image with α_2 axes, but sees no symmetry in the other image. Contributions are negative for this subject when seeing an axis of symmetry for the image with α_1 axes, but no symmetry in the other image. The signs of the contributions are inverted if the subject prefers complexity. We also approximate these contributions with their average:

$$D_{j,i}(\alpha_1, \alpha_2) = L \times \begin{cases} \left(1 - P_d^{j,i}(\alpha_1)\right) P_d^{j,i}(\alpha_2) - P_d^{j,i}(\alpha_1)\left(1 - P_d^{j,i}(\alpha_2)\right) & j > n_j^{(c)} \\ P_d^{j,i}(\alpha_1)\left(1 - P_d^{j,i}(\alpha_2)\right) - \left(1 - P_d^{j,i}(\alpha_1)\right) P_d^{j,i}(\alpha_2) & j \le n_j^{(c)} \end{cases}, \tag{10}$$

where we obtain $P_d^{j,i}(\alpha)$ from Equation (9), $n_j^{(c)}$ from Equations (7) and (8), and $1 - P_d^{j,i}(\alpha)$ represents failure of detection.

The only thing missing to specify the model fully is how to assign a value to $P_d^{j,i}(1)$. This value can be, in principle, any real number between 0 and 1. We thus looked for a low-parametric, behaviorally rich, continuous, monotonic probability distribution supported on a bounded interval. A good candidate was the continuous Bernoulli distribution [48]. This distribution is a one-parameter exponential family used in probability theory, statistics, and machine learning. Here, we used the distribution as follows:

$$P\left(P_d^{j,i}(1) : \lambda, \rho\right) = C(\lambda)\lambda^{P_d^{j,i}(1)/\rho}(1 - \lambda)^{1 - P_d^{j,i}(1)/\rho}, \tag{11}$$

where $0 < \lambda < 1$ is a constant parameter, $0 \le P_d^{j,i}(1)/\rho \le 1$, and $C(\lambda)$ is the normalization constant of the distribution. Therefore, in our usage of the distribution, $0 \le P_d^{j,i}(1) \le \rho$, that is, the parameter ρ expresses a limit in the range of $P_d^{j,i}(1)$. We chose ρ to be the limit of $P_d^{j,i}(1)$ because of the results in our first computational model. Those results show that $\rho < 1$. This limit of ρ is consistent with the second part of Assumption 3 in our theoretical framework. Because we obtained ρ through the fits from our first computational model, this parameter was not free in fits involving Equation (11).

4.4.3. Methods of Computer Simulations

The model has two free parameters that we can optimize and five fixed parameters. The free parameters are f_s and λ. In turn, because we want to simulate the results of Figure 4C–E, the fixed parameters had to include $N = 25$, $\alpha = \{0, 1, 2\}$, and $L = 60$. Moreover, parameter ρ is not free because we optimize it in our first computational model. Here, we set $\rho = 0.8$ because this value is just higher the one that we have found in that section. Smaller values of ρ found in that section are taken care of by this choice because $P_d^{j,i}(1) < \rho$. Low $P_d^{j,i}(1)$ correspond to a weak detection of axes of symmetry, which is

exactly what small values of parameter ρ do. Another fixed parameter that is not part of the optimization is the number of times that we repeat an experiment while keeping all the parameters constant. This parameter is $M = \{1000, 10,000, 30,000\}$.

In the most basic simulations, we fixed the free parameters f_s and λ, and calculated $D_{j,i}(0,1)$, $D_{j,i}(0,2)$, and $D_{j,i}(1,2)$ to capture the outcomes in Figure 4C–E. The algorithm for this calculation was as follows:

a. Sample $n_i^{(s)}$ from Equation (7).
b. Calculate $n_i^{(c)}$ from Equation (8) using the outcome from Step a.
c. Sample $P_d^{j,i}(1)$ from Equation (11).
d. Calculate $P_d^{j,i}(\alpha_1)$ and $P_d^{j,i}(\alpha_2)$ from Equation (9) using the outcome from Step c.
e. Calculate $D_{j,i}(\alpha_1, \alpha_2)$ from Equation (10) using the outcomes from Steps b and d.

Consequently, $D_{j,i}(\alpha_1, \alpha_2)$ depends on the free parameters f_s and λ, that is,

$$PD_{j,i}(\alpha_1, \alpha_2) = D_{j,i}(\alpha_1, \alpha_2 : f_s, \lambda), \tag{12}$$

In the simulations, we optimized the free parameters under different conditions to capture the outcomes in Figure 4C–E. The optimization followed a strategy similar to that of Equation (6). To do this, we measured the χ_i^2 of the goodness of fit of $D_{j,i}(\alpha_1, \alpha_2)$ (Equation (10)) to the equivalent data from Experiment 2 (Figure 4C–E), labeled $E_j(\alpha_1, \alpha_2)$:

$$\chi_i^2 = \sum_{j=0}^{N} \frac{\left(E_j(0,1) - D_{j,i}(0,1)\right)^2}{D_{j,i}(0,1)} + \frac{\left(E_j(0,2) - D_{j,i}(0,2)\right)^2}{D_{j,i}(0,2)} + \frac{\left(E_j(1,2) - D_{j,i}(1,2)\right)^2}{D_{j,i}(1,2)}.$$

The measure χ_i^2 depends on the free parameters of $D_{j,i}$ (Equation (12)), that is:

$$\chi_i^2 = \chi_i^2(f_s, \lambda).$$

To find the optimal free parameter set, we calculated:

$$\left(f_s^{(opt)}, \lambda^{(opt)}\right) = argmin_{f_s, \lambda} med_i\left(\chi_i^2(f_s, \lambda)\right), \tag{13}$$

where med_i represented the median of χ_i^2 for $1 \leq i \leq M$. Equation (13) employed the median because the distribution of χ_i^2 was not normal and, thus, we needed a robust estimator. As for Equation (6), we performed the minimization specified in Equation (13) with a coordinate descent algorithm. In some cases, we performed the optimization by fixing one of the two free parameters and optimizing with respect to the other one.

Because we measured the χ_i^2 statistic, we could use a goodness of fit test for the null hypothesis that the model fit data by chance. The number of degrees of freedom for this test was $3 \times N - 1 - 2 = 72$. The "2" in this equation was obtained from the number of free parameters in the model (Equation (13)). Alternatively, we plotted the predictions of the model against the experimental results, measuring the Pearson's correlation coefficient. We then tested the null hypothesis that the true correlation coefficient was equal to zero, based on the value of the sample correlation coefficient.

4.4.4. Results

The results from Experiment 2 showed that people who like symmetry preferred seeing two axes of it than just one. In turn, Experiment 1 demonstrated that seeing two axes of symmetry required temporal integration. Therefore, the preference for multiple axes of symmetry had to depend on the spatiotemporal integration of the image. The simplest form of integration arose in the scanning of the image by saccades or shifts of visual attention, possibly leading to a probability summation. The outcome of Experiment 3 supported this hypothesis for individual observers, supporting a model compatible with the assumptions in our theoretical framework. Here, we wanted to extend this model to

quantify its parameters in the population (Equations (7)–(11)). The results of this extension appear in Figure 6.
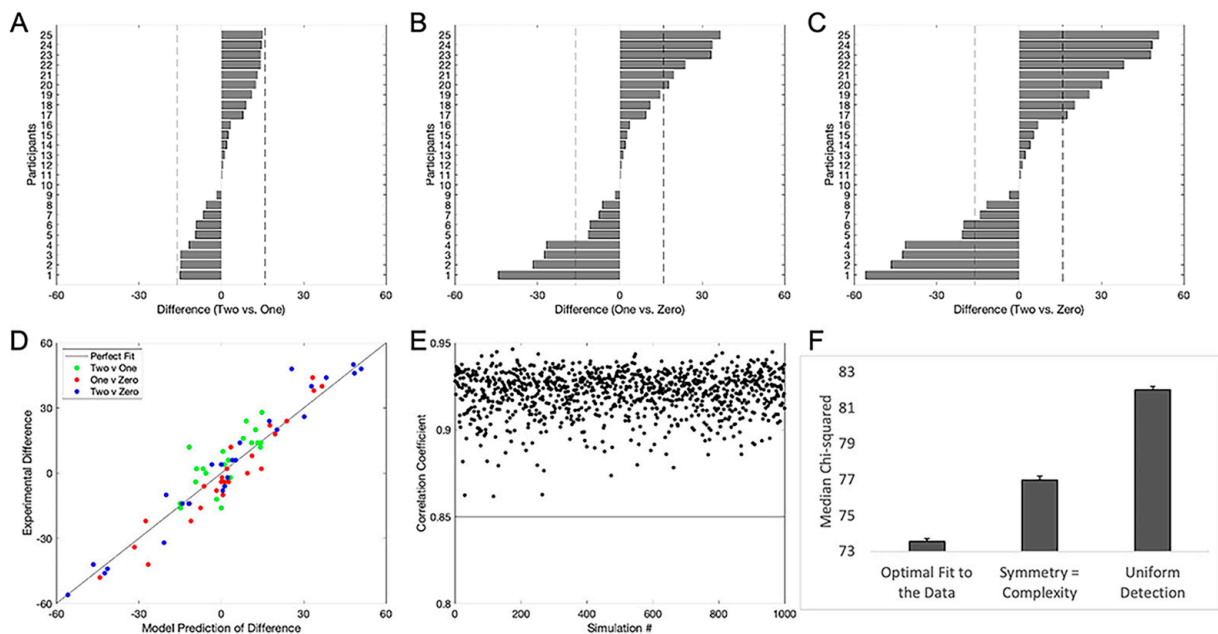

Figure 6. Results of the simulations with a population computational Model. (**A**–**C**) Graphical representation of individual differences in symmetry preference. These panels correspond and have the same conventions as (**D**,**E**) in Figure 4. We obtained these panels for the optimal model in the χ^2 sense with 30,000 simulations. (**D**) Experimental versus model-predicted differences for the same optimal model and in Panels (**A**–**C**). (**E**) Pearson's correlation coefficients for the best χ^2 model over 1000 simulations. (**F**) Median χ^2 over 30,000 simulations for the general optimal parameters (first bin), optimal parameters with $f_s = 1/2$ (second bin), and optimal parameters with $\lambda = 1/2$ (third bin). These plots indicate that the proposed computational model provides an excellent fit to the data.

Figure 6 shows that the computational model can provide good fits to the population data. A comparison of Figure 6A–C with Figure 4C–E shows a strong qualitative resemblance between model behavior and data. For example, take the images compared in Figure 6A,B. Although these images had the same difference in the number of axes of symmetry (one versus zero or two versus one), preferences were strong for Figure 6B, but weak for Figure 6A. In another example, adding one axis of symmetry increased the strength of preference (compare Figure 6C with Figure 6B). However, the preference did not just increase for symmetry. Those people who "disliked" symmetry became even more biased against it in both data (Figure 4) and model (Figure 6).

The goodness of fit of the model was not just limited to qualitative aspects. For example, Figure 6D plots the experimental results against the predictions of the model for the optimal fit in the χ^2 sense with 30,000 simulations using the optimal parameters. The optimal parameters were $f_s = 0.58$ and $\lambda = 0.094$. With these parameters, the optimal fit was good as judged by the proximity of the points to the line of a slope of 1 and intercept of 0. Indeed, the fit was indistinguishable from the data using the χ^2 goodness-of-fit test. The Pearson's correlation coefficient of the plot was also high ($r = 0.946$) and unlikely to increase by chance from a distribution with a zero correlation ($p < 0.01$). Finally, the correlation was high and the fit good for each of the individual conditions separately (Figure 6D).

Importantly, the goodness of the model fit was not limited to the optimal simulation in the χ^2 sense. Figure 6E shows the Pearson's correlation coefficients for a sequence of 1000 simulations using the optimal parameters. As the figure reveals, none of the correlation coefficients are less than 0.85. The median correlation coefficient over

these 1000 simulations is 0.9232 ± 0.0004 (standard error). Over the 30,000 simulations, most fits are undistinguishable from the data using the χ^2 goodness-of-fit test. Of these 30,000 simulations, only 14.4% can be distinguished from the data with this test at the $p < 0.001$ level.

4.4.5. Discussion

With such a good model, we reach two conclusions: first, as mentioned above, the optimal parameters of the model include $f_s = 0.58$. This optimal parameter suggests that more people ($60\% \pm 10\%$) prefer symmetry over complexity. (This $\pm 10\%$ estimate comes from the binomial distribution with N = 25 and $p = 0.6$). To test this suggestion further, we optimize the parameters again, but by constraining $f_s = 1/2$. The results in Figure 6F show that the fit is significantly better if we allow $f_s > 1/2$ (compare the two first bins in the figure). Our sample is too small to rule out $f_s = 1/2$; however, the data do indeed provide evidence that more people prefer symmetry to complexity. Second, the optimal parameters include $\lambda = 0.094$, which, by plotting Equation (11), yields a monotonically declining $P\left(P_d^{j,i}(1) : \lambda, \rho\right)$. This decline suggests that more people have difficulty detecting an axis than can find it with ease in our images. This suggestion is strongly supported by the results of Experiment 3 (Figure 5). To test this suggestion further, we optimize the parameters again, but by constraining $\lambda = 1/2$. With λ, $P\left(P_d^{j,i}(1) : \lambda, \rho\right)$ is a uniform distribution. The results in Figure 6F show that the fit is significantly better if we allow $\lambda < 1/2$ (compare the first and third bins in the figure). Again, our sample is too small to rule out $\lambda = 1/2$; however, the data show that detecting an axis of symmetry with our images is difficult.

Despite its good quality, the model is not perfect. For example, an analysis of Figure 6F shows that the optimal fit in the χ^2 sense may yield a slightly larger-than-one slope for the zero-versus-one condition (red dots). In addition, the Pearson's correlation coefficients are not as high for the one-versus-two condition (median $r = 0.7610 \pm 0.0002$). For the other conditions, these coefficients are above 0.9 (zero-vs-one median $r = 0.9245 \pm 0.0001$; zero-versus-two median $r = 0.9570 \pm 0.0001$). Furthermore, none of the differences for the one-versus-two condition crossed the statistical threshold in Figure 6A. However, these statistical deficiencies are minor and have simple explanations. For example, the range of values for the one-versus-two condition is small (green dots in Figure 6D), making their correlation coefficients more sensitive to noise. Consequently, overall, the model provided a good fit to the population data, allowing us to explore their meanings more thoroughly.

5. General Discussion

5.1. Time Required for the Detection of Multiple Axes of Symmetry

Our experiments suggest that time has a significant effect on symmetry detection. While participants cannot detect multiple embedded axes of symmetry at 300 milliseconds, they can detect them at a 1 s interval. Thus, detecting multiple axes of symmetry takes time, and our results suggest that slower mechanisms are responsible for this detection. One of these possible explanatory mechanisms is eye movement, especially, saccades. The time between stimulus presentation and the onset of a saccadic movement is thought to be, on average, 200 milliseconds [36]. Our results indicate that participants may be shifting their gaze, and this is what may be allowing them to detect multiple axes of symmetry at longer intervals. Another possible explanatory long-interval mechanism is a shift in visual attention. The latency of visual attention is thought to be between 140 and 240 milliseconds [37]. Again, our results suggest that participants may be shifting their visual attention to detect multiple vertical axes of symmetry embedded in noise. Moreover, because the detection of multiple axes appears to depend on slower mechanisms scanning the image, our results support the neuroscientific claims that extrastriate brain areas mediate the perception of symmetry. These are areas with large receptive fields [21,22].

5.2. Why People like Multiple Axes of Symmetry

Because the detection of multiple axes of symmetry required a long temporal integration, we initially hypothesized that they would not have a positive effect on preference. The rationale for this hypothesis was the simplest application of the processing fluency theory [7,29]. However, our data did not support this hypothesis. We saw two possible explanations for why our data showed an effect of multiple axes of symmetry on preference through temporal integration. One possible explanation could be the temporal integration of symmetry value. For example, imagine that participants detected one axis and assigned it a value rating. Upon detecting a second axis (potentially through an eye shift or a shift in attention), they assigned to that axis another value rating. This new value rating would then be integrated with the first value rating, and the accumulation of value would determine their preference response. Therefore, the time course of preference accumulation would have to be longer than the time it took to detect a second axis after having detected one. However, this accumulation should be sublinear as a function of the number of axes because a biased preference was reduced for the two-versus-one condition when compared to the zero-versus-one alternative. If the accumulation was instead proportional to the number of axes, then the two conditions should have yielded similar results.

Another explanation for the effect of multiple axes of symmetry on preference through temporal integration is probability summation [44]. Thus, the scanning performed by saccades or shifts of attention would be used to try to detect at least one axis of symmetry. If finding one axis is enough, this would explain the weak preference bias for the one-versus-two condition compared to the zero-versus-one condition. In the former, at least one axis of symmetry could be found in both images, eliminating the preference bias when that occurred. This process is probability summation because it uses the probability of detecting at least on axis when several are present. This probability-summation process is the basis of the computational model proposed in this article. The success of this model suggests that the brain employs such a process when dealing with multiple axes of symmetry. Interestingly, the model is compatible with the processing fluency theory. Although detecting multiple axes of symmetry takes time, detecting a single axis is quick [12,24,49] and has dedicated cortical circuitry [13–15].

5.3. Do People Always Prefer Symmetry?

However, we did not obtain a statistically significant preference of one-over-zero axes of symmetry. This statistical failure occurred even if the opposite held for the two-over-zero (and two-over-one) axes of symmetry. The apparent neutrality of the one-over-zero case went against the research suggesting that people preferred symmetry over asymmetry [1,3]. We conceive three factors that may have contributed to the statistical neutrality of the one-over-zero cases and its absence in two-over-zero situations. First, both saliency and attention affect the preference for symmetry in abstract patterns. The saliency of symmetry in abstract patterns is positively correlated with preference [50,51]. However, in some cases, abstract symmetrical patterns are associated with a positive affect only when the task involves symmetry detection [49]. In our experiments, images with two embedded axes (as opposed to one) doubled the probability of participants detecting one of them, and therefore possibly preferring the stimuli. Second, statistics may have contributed to the apparent neutrality of the one-over-zero case. The pattern of preference was consistent for individual participants when comparing both the difference between zero and one and zero and two axes (Figure 4F–H). Thus, having two axes might have increased the magnitude of the effect to the point of statistical significance. Third, while some people preferred symmetrical images over more complex ones, others liked the opposite. This surprising split of preference for symmetry was strongly supported by data, such as those in Figure 5D,E. Hence, as a population, people are split into these two categories of preference. This split reduces the mean strength of preference for images with single axes of symmetry. The findings of our computational model lend credibility to the second and third explanations above.

A key finding of our results is the role of individuality in aesthetic preference. Studies on symmetry preference tend to average across participants. Our study shows that, as a population, people prefer symmetry over complexity. However, our results show a distinction between individuals when it comes to symmetry and complexity preferences. Some people significantly like symmetry over complexity and others prefer the opposite (Figure 5D,E). Based on the optimal fit of our computational model, 15 ± 2.4 participants ($60 \pm 10\%$) are in the symmetry-preferring category, while 10 ± 2.4 ($40 \pm 10\%$) are in the second. The model also reveals another important source of individuality. The optimal parameter related to detectability of an axis of symmetry, λ, suggests strong individuality in the ease to detect symmetry. Thus, the detectability of symmetry varies across individuals, affecting their preferences. These results support the notion that individual differences in aesthetic preferences cannot be ignored, highlighting the limits of generalizing about aesthetic preferences based on group means [52].

References

1. Rodríguez, I.; Gumbert, A.; Hempel de Ibarra, N.; Kunze, J.; Giurfa, M. Symmetry Is in the Eye of the 'Beeholder': Innate Preference for Bilateral Symmetry in Flower-Naïve Bumblebees. *Naturwissenschaften* **2004**, *91*, 374–377. [CrossRef] [PubMed]
2. Treder, M.S. Behind the Looking-Glass: A Review on Human Symmetry Perception. *Symmetry* **2010**, *2*, 1510–1543. [CrossRef]
3. Wenderoth, P. The Salience of Vertical Symmetry. *Perception* **1994**, *23*, 221–236. [CrossRef]
4. Palmer, S.E.; Schloss, K.B.; Sammartino, J. Visual Aesthetics and Human Preference. *Annu. Rev. Psychol.* **2013**, *64*, 77–107. [CrossRef]
5. Tinio, P.P.L.; Leder, H. Just How Stable Are Stable Aesthetic Features? Symmetry, Complexity, and the Jaws of Massive Familiarization. *Acta Psychol.* **2009**, *130*, 241–250. [CrossRef]
6. Voloshinov, A.V. Symmetry as a Superprinciple of Science and Art. *Leonardo* **1996**, *29*, 109–113. [CrossRef]
7. Aleem, H.; Correa-Herran, I.; Grzywacz, N.M. Inferring Master Painters' Esthetic Biases from the Statistics of Portraits. *Front. Hum. Neurosci.* **2017**, *11*, 94. [CrossRef]
8. Nucci, M.; Wagemans, J. Goodness of Regularity in Dot Patterns: Global Symmetry, Local Symmetry, and Their Interactions. *Perception* **2007**, *36*, 1305–1319. [CrossRef]
9. Bichot, N.P.; Rossi, A.F.; Desimone, R. Parallel and Serial Neural Mechanisms for Visual Search in Macaque Area V4. *Science* **2005**, *308*, 529–534. [CrossRef]
10. Shipp, S. The Brain Circuitry of Attention. *Trends Cogn. Sci.* **2004**, *8*, 223–230. [CrossRef]

11. Sigman, M.; Dehaene, S. Brain Mechanisms of Serial and Parallel Processing during Dual-Task Performance. *J. Neurosci.* **2008**, *28*, 7585–7598. [CrossRef] [PubMed]
12. Wagemans, J.; Van Gool, L.; D'ydewalle, G. Detection of Symmetry in Tachistoscopically Presented Dot Patterns: Effects of Multiple Axes and Skewing. *Percept. Psychophys.* **1991**, *50*, 413–427. [CrossRef] [PubMed]
13. Sasaki, Y.; Vanduffel, W.; Knutsen, T.; Tyler, C.; Tootell, R. Symmetry Activates Extrastriate Visual Cortex in Human and Nonhuman Primates. *Proc. Natl. Acad. Sci. USA* **2005**, *102*, 3159–3163. [CrossRef] [PubMed]
14. Tyler, C.W.; Baseler, H.A.; Kontsevich, L.L.; Likova, L.T.; Wade, A.R.; Wandell, B.A. Predominantly Extra-Retinotopic Cortical Response to Pattern Symmetry. *Neuroimage* **2005**, *24*, 306–314. [CrossRef]
15. Cattaneo, Z. The Neural Basis of Mirror Symmetry Detection: A Review. *J. Cogn. Psychol.* **2017**, *29*, 259–268. [CrossRef]
16. Chen, C.-C.; Kao, K.-L.C.; Tyler, C.W. Face Configuration Processing in the Human Brain: The Role of Symmetry. *Cereb. Cortex* **2007**, *17*, 1423–1432. [CrossRef]
17. Saarinen, J.; Levi, D.M. Perception of Mirror Symmetry Reveals Long-Range Interactions between Orientation-Selective Cortical Filters. *NeuroReport* **2000**, *11*, 2133–2138.
18. Tyler, C.W.; Hardage, L.; Miller, R.T. Multiple Mechanisms for the Detection of Mirror Symmetry. *Spat. Vis.* **1995**, *9*, 79–100.
19. Tyler, C.W.; Hardage, L. Mirror Symmetry Detection: Predominance of Second-Order Pattern Processing throughout the Visual Field. In *Human Symmetry Perception and Its Computational Analysis*; Psychology Press: London, UK, 2002; ISBN 978-1-4106-0660-0.
20. Desimone, R.; Gross, C.G. Visual areas in the temporal cortex of the macaque. *Brain Res.* **1979**, *178*, 363–380.
21. Smith; Singh, K.D.; Williams, A.L.; Greenlee, M.W. Estimating Receptive Field Size from FMRI Data in Human Striate and Extrastriate Visual Cortex. *Cereb. Cortex* **2001**, *11*, 1182–1190. [CrossRef]
22. Olivers, C.N.L.; van der Helm, P.A. Symmetry and Selective Attention: A Dissociation between Effortless Perception and Serial Search. *Percept. Psychophys.* **1998**, *60*, 1101–1116. [CrossRef] [PubMed]
23. Pramod, R.T.; Arun, S.P. Symmetric objects become special in perception because of generic computations in neurons. *Psychol. Sci.* **2018**, *29*, 95–109. [PubMed]
24. Tyler, C.W. The Symmetry Magnification Function Varies with Detection Task. *J. Vis.* **2001**, *1*, 7. [CrossRef] [PubMed]
25. Dakin, S.C.; Herbert, A.M. The Spatial Region of Integration for Visual Symmetry Detection. *Proc. R. Soc. Lond. Ser. B Biol. Sci.* **1998**, *265*, 659–664. [CrossRef]
26. Strasburger, H. Seven Myths on Crowding and Peripheral Vision. *i-Perception* **2020**, *11*, 2041669520913052. [CrossRef]
27. Traquair, H.M. *An Introduction to Clinical Perimetry*; Henry Kimpton Publisher: London, UK, 1927.
28. Aleem, H.; Pombo, M.; Correa-Herran, I.; Grzywacz, N.M. Is Beauty in the Eye of the Beholder or an Objective Truth? A Neuroscientific Answer. In *Mobile Brain-Body Imaging and the Neuroscience of Art, Innovation and Creativity*; Contreras-Vidal, J.L., Robleto, D., Cruz-Garza, J.G., Azorín, J.M., Nam, C.S., Eds.; Springer Series on Bio- and Neurosystems; Springer International Publishing: Cham, Switzerland, 2019; pp. 101–110, ISBN 978-3-030-24326-5.
29. Reber, R.; Schwarz, N.; Winkielman, P. Processing Fluency and Aesthetic Pleasure: Is Beauty in the Perceiver's Processing Experience? *Pers. Soc. Psychol. Rev.* **2004**, *8*, 364–382. [CrossRef]
30. Cohen, J. *Statistical Power Analysis for the Behavioral Sciences*, 2nd ed.; L. Erlbaum Associates: Hillsdale, NJ, USA, 1988; ISBN 978-0-8058-0283-2.
31. Champely, S. *Pwr: Basic Functions for Power Analysis*; R Package Version 1.3-0; 2020. Available online: https://cran.r-project.org/web/packages/pwr/.
32. Correll, J.; Mellinger, C.; McClelland, G.H.; Judd, C.M. Avoid Cohen's 'Small', 'Medium', and 'Large' for Power Analysis. *Trends Cogn. Sci.* **2020**, *24*, 200–207. [CrossRef]
33. Peirce, J.; Gray, J.R.; Simpson, S.; MacAskill, M.; Höchenberger, R.; Sogo, H.; Kastman, E.; Lindeløv, J.K. PsychoPy2: Experiments in Behavior Made Easy. *Behav. Res.* **2019**, *51*, 195–203. [CrossRef]
34. Hunter, J.D. Matplotlib: A 2D Graphics Environment. *Comput. Sci. Eng.* **2007**, *9*, 90–95. [CrossRef]
35. R Core Team. *R: A Language and Environment for Statistical Computing*; R Foundation for Statistical Computing: Vienna, Austria, 2013. Available online: http://www.R-project.org/.
36. Miller, D. Saccadic and Pursuit Systems: A Review. *J. Pediatr. Ophthalmol. Strabismus* **1968**, *5*, 39–43. [CrossRef]
37. Carlson, T.A.; Hogendoorn, H.; Verstraten, F.A.J. The Speed of Visual Attention: What Time Is It? *J. Vis.* **2006**, *6*, 6–11. [CrossRef]
38. Aleem, H.; Correa-Herran, I.; Grzywacz, N.M. A Theoretical Framework for How We Learn Aesthetic Values. *Front. Hum. Neurosci.* **2020**, *14*, 345. [CrossRef]
39. Donderi, D.C. An Information Theory Analysis of Visual Complexity and Dissimilarity. *Perception* **2006**, *35*, 823–835. [CrossRef]
40. Correa-Herran, I.; Aleem, H.; Grzywacz, N.M. Evolution of Neuroaesthetic Variables in Portrait Paintings throughout the Renaissance. *Entropy* **2020**, *22*, 146. [CrossRef] [PubMed]
41. Güçlütürk, Y.; Jacobs, R.H.A.H.; van Lier, R. Liking versus Complexity: Decomposing the Inverted U-Curve. *Front. Hum. Neurosci.* **2016**, *10*, 112. [CrossRef] [PubMed]
42. Tyler, C.W.; Chen, C.-C. Signal Detection Theory in the 2AFC Paradigm: Attention, Channel Uncertainty and Probability Summation. *Vis. Res.* **2000**, *40*, 3121–3144. [CrossRef]
43. Andrews, L.C. *Special Functions of Mathematics for Engineers*; SPIE Press: Bellingham, WA, USA, 1998; ISBN 978-0-8194-2616-1.
44. Pombo, M.; Brielmann, A.A.; Pelli, D.G. The Intrinsic Variance of Beauty Judgment. *Atten. Percept. Psychophys.* **2022**, *85*, 1355–1373.

45. Rousseeuw, P.J.; Leroy, A.M. *Robust Regression and Outlier Detection*; Wiley Series in Probability and Mathematical Statistics; Wiley: New York, NY, USA, 1987; ISBN 978-0-471-85233-9.
46. Nelder, J.A.; Mead, R. A Simplex Method for Function Minimization. *Comput. J.* **1965**, *7*, 308–313. [CrossRef]
47. Wright, S.J. Coordinate Descent Algorithms. *Math. Program.* **2015**, *151*, 3–34. [CrossRef]
48. Loaiza-Ganem, G.; Cunningham, J.P. The Continuous Bernoulli: Fixing a Pervasive Error in Variational Autoencoders. *Adv. Neural Inf. Process. Syst.* **2019**, *32*, 13287–13297.
49. Bertamini, M.; Makin, A.; Pecchinenda, A. Testing Whether and When Abstract Symmetric Patterns Produce Affective Responses. *PLoS ONE* **2013**, *8*, e68403. [CrossRef]
50. Makin, A.D.J.; Wright, D.; Rampone, G.; Palumbo, L.; Guest, M.; Sheehan, R.; Cleaver, H.; Bertamini, M. An Electrophysiological Index of Perceptual Goodness. *Cereb. Cortex* **2016**, *26*, 4416–4434. [CrossRef] [PubMed]
51. Bertamini, M.; Rampone, G.; Makin, A.D.J.; Jessop, A. Symmetry Preference in Shapes, Faces, Flowers and Landscapes. *PeerJ* **2019**, *7*, e7078. [CrossRef] [PubMed]
52. Pombo, M.; Pelli, D.G. Aesthetics: It's Beautiful to Me. *Curr. Biol.* **2022**, *32*, R378–R379. [CrossRef] [PubMed]